Advanced Materials Research
ISSN: 1662-8985, Vol. 1163, pp 73-88
doi:10.4028/www.scientific.net/AMR.1163.73

Submitted: 2020-05-09
Revised: 2020-10-23
Accepted: 2020-12-14
Online: 2021-04-28

Performance Comparison of Microchannel Heat Sink Using Boron-Based Ceramic Materials

Md Tanbir Sarowar[1,a]

[1]Department of Mechanical and Production Engineering, Islamic University of Technology, Board Bazar,1704, Bangladesh

[a]tanbirsarowar@iut-dhaka.edu

Keywords: Microchannel heat sink, Numerical analysis, Ultra-high temperature ceramics, Heat transfer modelling

Abstract. Microchannel heat sink plays a vital role in removing a considerable amount of heat flux from a small surface area from different electronic devices. In recent times, the rapid development of electronic devices requires the improvement of these heat sinks to a greater extent. In this aspect, the selection of appropriate substrate materials of the heat sinks is of vital importance. In this paper, three boron-based ultra-high temperature ceramic materials (ZrB_2, TiB_2, and HfB_2) are compared as a substrate material in a microchannel heat sink using a numerical approach. The fluid flow and heat transfer are analyzed using the finite volume method. The results showed that the maximum temperature of the heat source didn't exceed 355K at 3.6MWm^{-2} for any material. The results also indicated HfB_2 and TiB_2 to be more useful as a substrate material than ZrB_2. By applying 3.6 MWm^{-2} heat flux at the source, the maximum obtained surface heat transfer coefficient was 175.2 $KWm^{-2}K^{-1}$ in a heat sink having substrate material HfB_2.

Introduction

The recent advancements in micro-electro-mechanical systems (MEMS) have introduced a high demand for removing a considerable amount of heat flux from compact areas. With continuous improvements in semiconductors and high-density electronics circuits, the necessity of introducing efficient cooling techniques is ever increasing[1]. In many cases, an efficient cooling mechanism is one of the main obstacles in the advancements and miniaturization of these electronic circuits[1]. The high functioning electronic devices can produce more than 100 W/cm^2 heat flux[2]. For the effective operation of the electronic devices in most cases, their operating temperature should be maintained below 401K[3]. To remove this high amount of heat flux from a small area, the concept of the microchannel heat sink was first introduced by Tuckerman and Pease in 1981[4]. They pointed out that decreasing the dimension of the flow channel to a micron-scale can effectively increase the heat transfer rate. In that experiment, they used a heat sink with a groove width and fin width of 50 μm, which could attain a heat transfer rate up to 10 $Wcm^{-2}K^{-1}$. Following that, extensive research has been carried out on optimizing the MCHS for the best performance regarding the improvement of heat transfer at a lower pressure loss and other factors[5–8].

The optimization procedure of this kind of heat exchangers can be done in a number of ways. The first method can be regarded as the geometry optimization[9–12]. The geometry optimization contains different channel shapes[5,13–16], and also choosing between single or double-layer sink configurations[17–22]. Another effective method is the selection of optimum working fluid to run through the microchannels. Hadad et al.[23] mentioned using water is more suitable than air as a cooling medium. Another advancement in this field is the introduction of the nanofluids. Jang et al. [8] used nanofluids such as 6 nm copper-in-water and 2 nm diamond-in-water. They showed that at the fixed pumping power of 2.25W, the performance of the heat sink was improved 10% compared to a microchannel heat sink using water. Similarly, many works have been reported using different nanofluids in microchannel heat sinks[7,24–27].

Another aspect of improving heat transfer performance is the selection of appropriate material for the heat sink's substrate. It can be noted that with a comparison with the geometry optimization and working fluid selection, the number of studies is very limited in this aspect[28,29]. Conventionally,

the micro-channel heat sink is manufactured by metals and metal alloys[28]. Kang et al.[30] analyzed a microchannel heat using silicon. Kuznetsov et al.[31] used copper microchannels for their analysis. Dang et al.[32] used aluminum as the material for their studies. But using these metals or metal alloys are limited at high temperatures, especially up to 800^0C[6,32–36]. Ceramic materials can be suitable alternatives in this aspect[37–42]. These materials can withstand a higher temperature than metals without showing any deformations[43,44]. The obstacle that remains is the lower thermal conductivity of these materials[45]. And for using a material in a micro-channel heat sink, having an excellent thermal conductivity is very much needed. However, few advanced ceramics such as ZrB_2[46–54], TiB_2[55–58], HfB_2[46,55,59–61] possess high thermal conductivities as well as excellent physical properties.

Carmen et al.[62] applied a ceramic made microchannel heat exchanger on a microturbine. They showed silicon carbon nitride (SiCN) ceramic, as a stable material at temperatures up to 1300^0C, in a combustion gases media. Nagarajan et al.[63] studied a ceramic plate-fin exchanger fabricated by silicon-carbide (SiC). Nekahi et al.[52] performed analysis on the thermal performance of a microchannel heat exchanger constructed by TiB_2–SiC and TiB_2–SiC doped carbon nanofibers (TiB2–SiC–C_f) materials. They found a heat transfer improvement of 15.7% and 15.5% utilizing TiB2–SiC and TiB2–SiC–C_f, compared to Al_2O_3, respectively. Fattahi et al.[64] used aluminum nitride (AlN) to perform numerical simulations on a plate heat exchanger. Their results showed a remarkable heat transfer enhancement of 59%, compared to the Al_2O_3 made one. Vajdi et al.[53] proposed a micro-channel heat sink made of ZrB_2, which could withstand 3.6 MW/m^2 by not exceeding the heat source temperature more than 360K with working fluid water at 250 Reynolds number.

The present study furthers the work done by Vajdi et al.[53] by introducing two other ultra-high temperature ceramic materials titanium diboride (TiB_2) and hafnium diboride (HfB_2), in manufacturing microchannel heat sink. These two materials show very similar thermal conductivities, as shown in figure 5 but slightly better than ZrB_2 in the range of the working temperature of heat sinks. But they possess quite different heat capacity values, as seen in figure 6. The present work compares these two other ceramic materials with ZrB_2 for introducing the most efficient one for manufacturing a heat sink.

Problem Description

The heat transfer and fluid flow inside a microchannel heat sink made by three different ceramic material is studied using the finite volume method. The geometry used for the simulation is illustrated in figure 1, which is based on experimental work done by [65]. The heat sink consists of rectangular channels having a dimension of 57×180μm. There are 110 channels with identical geometry constituating a length of 11mm. Since all the channels have the same geometry, similar heat transfer behavior can be found in all the channels. For computational advantages, only a single representative channel is selected for the computational model instead of investigating the whole MCHS. The working fluid considered is water having a temperature of T_0=293K at the inlet. Mass flow inlet boundary condition was considered at the inlet, and the outlet was selected as a pressure outlet. The bottom wall of the heat sink is introduced with constant heat flux. The top wall of the sink is assumed to be having an insulated wall for generating a closed domain for fluid flow. The detailed geometric information and the boundary conditions are shown in figure 1 and figure 2.

Geometric Model

The geometric model, as shown in figure 1, is used for the analysis. The channel dimension is 57×180μm. The length of the channels is the same as the length of the heat sink, which is 10mm. The geometry is modeled using Ansys ICEM CFD software. For computational advantages and similar fluid flow and heat transfer properties, one of the microchannels is selected for the analysis, as shown in figure 2.

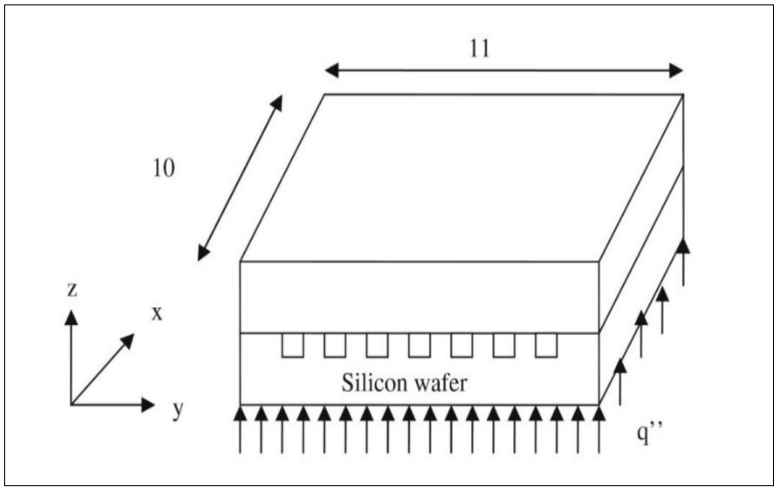

Figure 1. Structure of microchannel heat sink

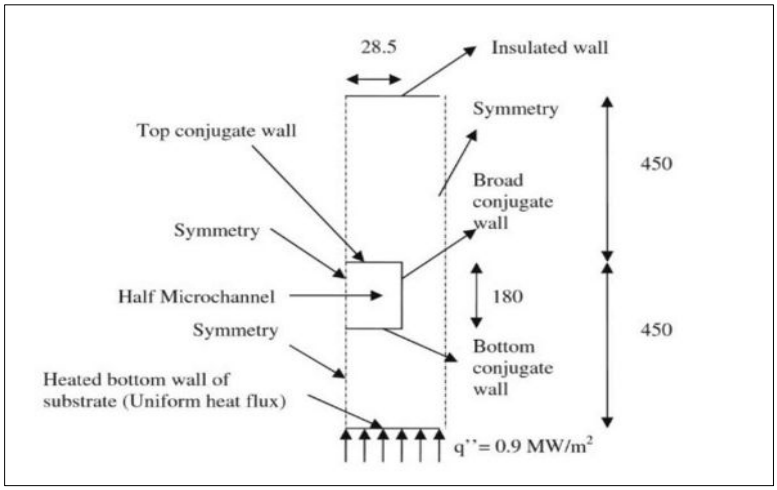

Figure 2. The geometry used for simulation (half channel)

Grid Generation

We know that the accuracy of the numerical analysis relies very much on the grid generation. The accuracy of the results increases with the increase in the number of cells used for the discretization of the domain. The results are also affected by the type of cell elements used, especially in the case of flow-through small channels like microchannel heat sinks (MCHS). For the present analysis, tetrahedral cell elements are used for the solid domain, which allows us to generate a finer mesh in regions closer to the fluid domain, as shown in the figures 3 and 4. Hexahedral cells are used for the fluid domain for capturing the flow physics such as thermal and hydrodynamic boundary layers more accurately.

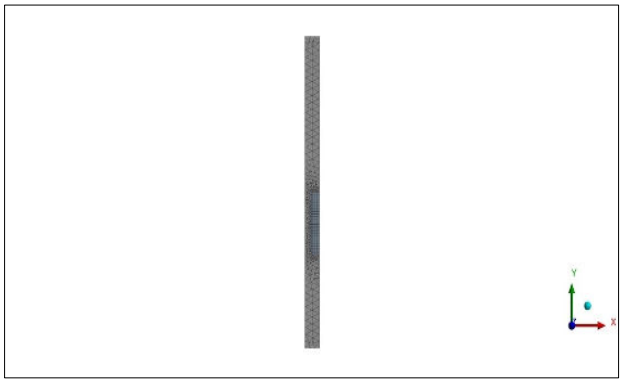

Figure 3. Front view of the grid

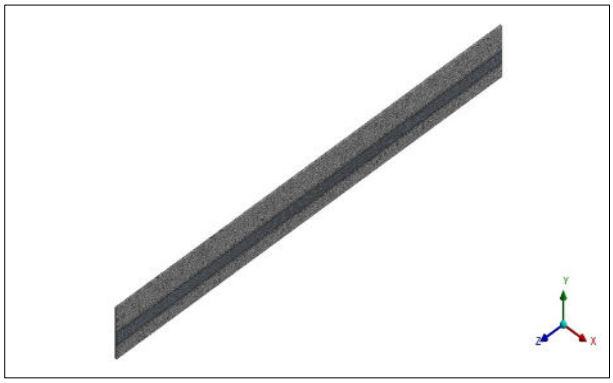

Figure 4. Isometric view of the grid

Governing Equations

The governing equations are the standard continuity equation for conservation of mass, Navier-Stokes equation for conservation of momentum, and the energy equation for predicting the conjugate heat transfer. During the analysis, the following assumptions are being made:

(1) Steady-state fluid flow and heat transfer
(2) Flow is incompressible
(3) Laminar flow
(4) Radiative heat transfer is negligible
(5) No-slip boundary conditions for the inner wall of the flow channels
(6) Constant fluid properties

By incorporating the assumptions mentioned, the following governing equations of the fluid flow and heat transfer are obtained:

– Conservation of mass (continuity):

$$\nabla . v = 0 \tag{1}$$

where, ν the is the velocity field and ∇ is the Nabla mathematical operator.

– Conservation of momentum:

$$\rho_f v . \nabla v = -\nabla p + \nabla . (\mu f \nabla v) \tag{2}$$

where, ρ_f is fluid density, p is the pressure, and μ_f is the fluid viscosity.

– Conservation of energy for fluid:

$$\rho_f C_{p,f} . \nabla T = \nabla . (k_f \nabla T) \tag{3}$$

where, $C_{p,f}$ is the fluid specific heat, T is the temperature, k_f is the fluid thermal conductivity.

– Conservation of energy for solid:

$$\nabla . (k_s \nabla T) = 0 \tag{4}$$

where, k_s the is the solid thermal conductivity.

Material Properties

Microchannel heat sinks are used to recover high heat flux from high functioning electronic devices having a minimal surface area. Thus, high heat flux removal causes the sink temperature to increase rapidly and to a larger value. This higher temperature might damage the heat sink if we don't use a durable material in manufacturing these heat removal devices. For which reason, ceramic materials can be a proper alternative for commonly used alloys or metals since these materials can work at high temperatures and, at the same time, can withstand the high resulted thermal stresses.

However, in spite of showing excellent resistive properties against corrosions issues, most of the ceramic materials show quite low thermal conductivity and heat capacity values which are the most important factor for any material to be used as a substrate for any heat sink. But ZrB_2, TiB_2, and HfB_2 possess a remarkably good thermal conductivity as well as heat capacity, as shown in figure 5 and figure 6 which allow us to use these ceramic materials in microchannel heat sink.

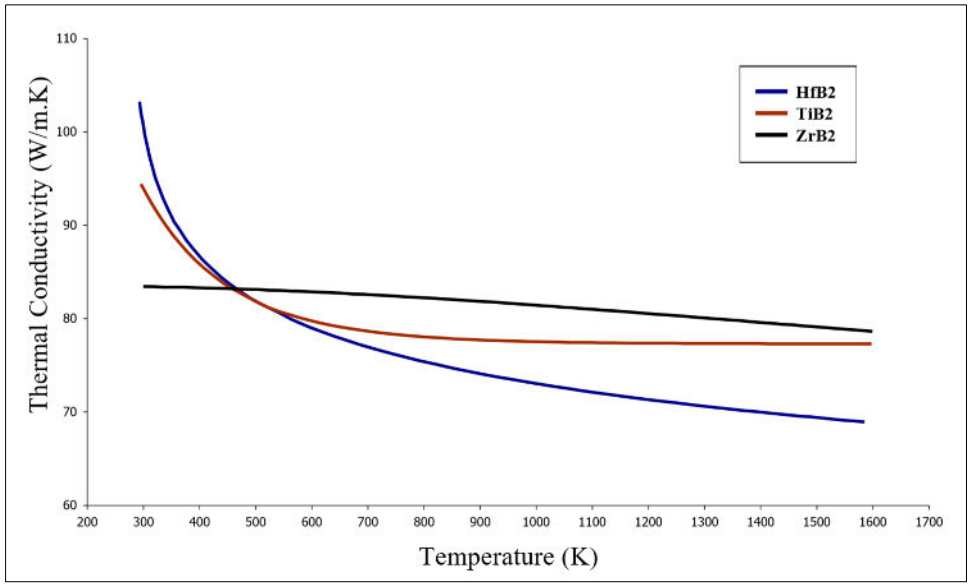

Figure 5. Thermal conductivity of ZrB_2[66], TiB_2[67], and HfB_2[46]

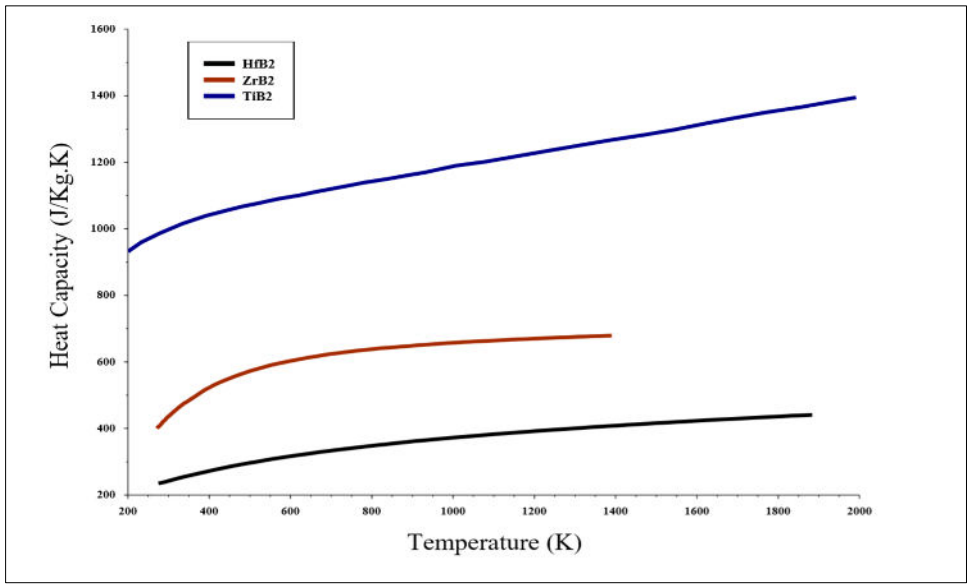

Figure 6. Heat capacity of ZrB_2[66], TiB_2[67], and HfB_2[46]

Solution Methodology

The governing equations of the fluid flow and heat transfer were solved by the finite volume method, which is based upon spatial integration of the governing equations over finite control volumes. Commercial CFD software package FLUENT version 17.0 has been used for the simulation. The solution was initialized by the boundary conditions, as mentioned in figure 2. The pressure-based steady-state 3D segregated solver has been used. The pressure-based solver uses a solution algorithm where the governing equations are solved sequentially. The conjugate boundary condition at solid-fluid interfaces ensures that the energy equation in solid and fluid zones are solved simultaneously. Temperature-dependent thermal conductivity and specific heat capacity of the materials are incorporated in the model using user-defined functions (UDF). Pressure-velocity coupling is done by SIMPLE (Semi Implicit Method for Pressure-Linked Equations) algorithm, which combines the continuity and momentum equations to derive the pressure-correction equation. The advective terms in momentum and energy equations are discretized by the second-order upwind scheme to contain the numerical errors. The entire domain was initialized with the conditions of the inlet boundary before starting the iterative process, where the reference zone was selected as fluid. Underrelaxation factors for the update of computed variables at each iteration are for pressure = 0.3,

momentum = 0.7 and energy = 1. Qualitative convergence has been judged by residual falling below 10^{-6} for continuity, energy, and the velocity components. The quantitative convergence is judged by maximum substrate temperature remaining unchanged with subsequent iterations.

Validation and Mesh Independence

The numerical model was validated against the work done by Bhattacharya et al.[65]. According to their analysis, the material used for the microchannel heat sink was silicon, and the working fluid was selected as water. The temperature of water at the inlet was 293K. The flow Reynolds number was 250. The bottom wall of the heat sink was introduced with a heat source of 0.9 MW/m^2. We can see the numerical model showed much agreement with the work presented in [65] as shown in figure 7. So, the numerical model can be used for further analyzing the heat transfer and fluid flow for the microchannel heat sink using different substrate materials. The results have also been validated against the number of elements of the generated mesh. It has been seen that the results seem independent of the number of elements beyond 0.6 million elements. The generated grid for the analysis contained 755105 elements.

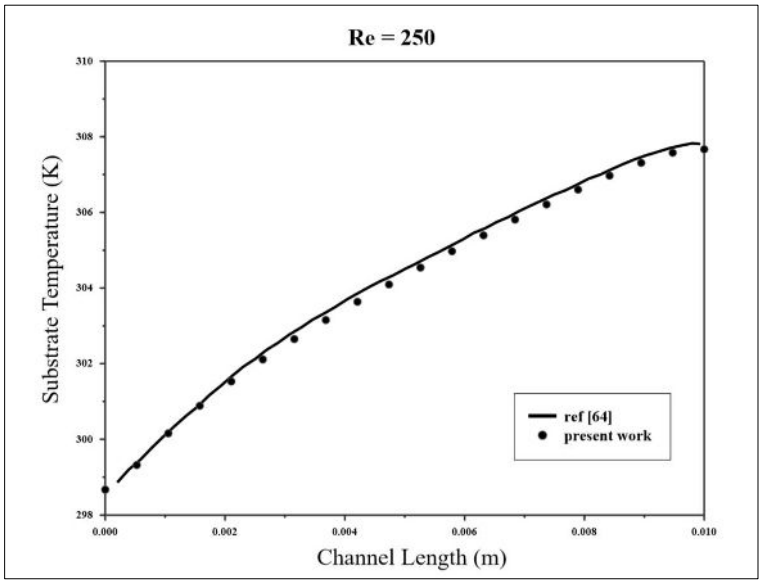

Figure 7. Substrate wall temperature comparison between present work and ref [64]

Results and Discussion

A three-dimensional steady-state numerical simulation has been performed on the same geometry, as presented by Bhattacharya et al.[65]. Three different boron-based ceramic materials named hafnium diboride (HfB_2), titanium diboride (TiB_2), and zirconium diboride (ZrB_2) are used as a substrate material for the microchannel heat sink. Four different heat fluxes are applied at the bottom wall of the heat sink. The working fluid flowing inside the channel is water having temperature at the inlet 293K. At first, the flow Reynolds number is kept 250 for the simulations changing the surface heat flux to obtain the substrate wall temperature.

We know the main goal of these micro-channel heat sinks is to maintain the temperature of the electronic devices below a specific value. That's why the temperature of the source of heat flux is plotted against the channel length for three different materials at different heat fluxes. We can see the maximum source temperature is maximum for ZrB_2, followed by TiB_2 and then HfB_2. Heat sinks having material HfB_2 and TiB_2 shows quite a similar temperature range at the substrate because of their quite similar thermal conductivity values within the range of the temperature at the heat sink. The results show that the maximum surface temperature occurs at the exit of the channel. Analyzing the temperature plots of figures 8, 9, and 10, we can see that applying different heat fluxes at the bottom of the heat sinks, the heat sink having ZrB_2 material shows maximum surface temperature followed by TiB_2 and then HfB_2.

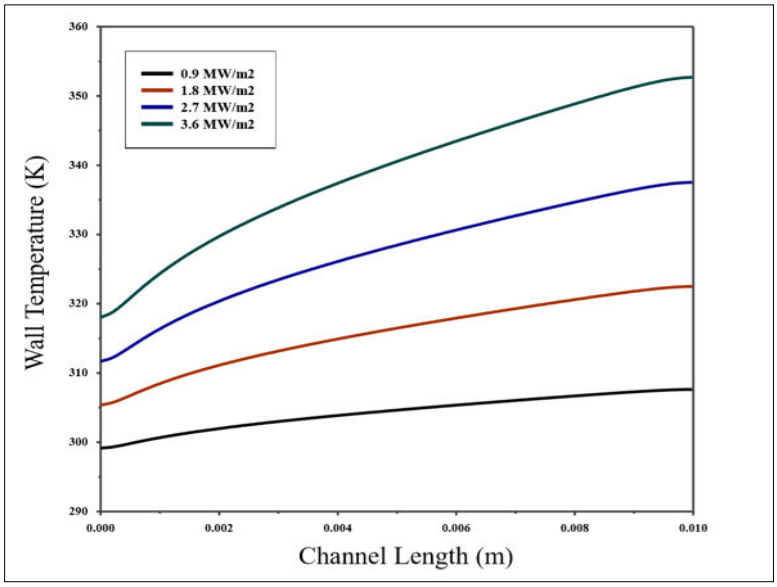

Figure 8. Substrate wall temperature vs. channel length for HfB_2

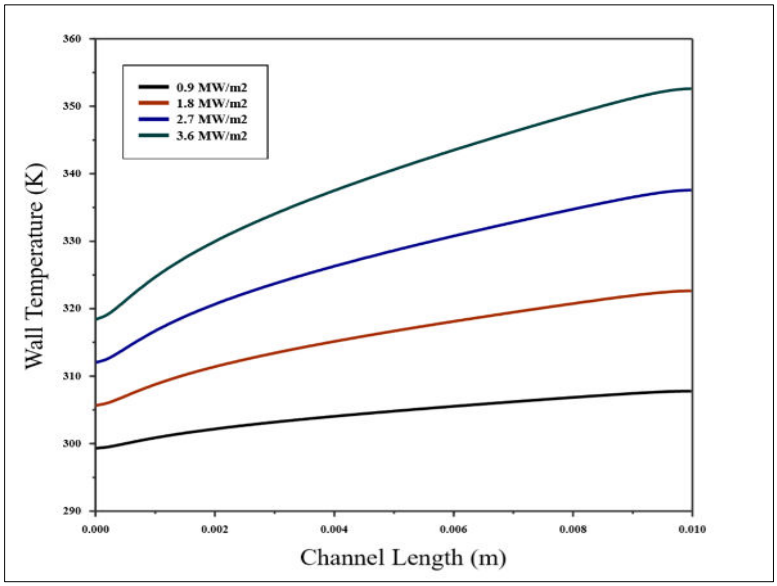

Figure 9. Substrate wall temperature vs. channel length for TiB_2

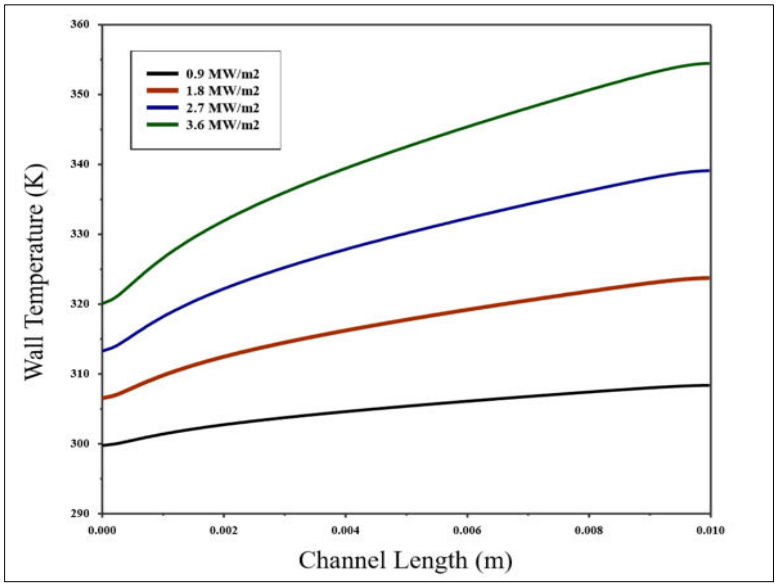

Figure 10. Substrate wall temperature vs. channel length for ZrB_2

Now, to compare the results obtained in the present study with literature, the maximum surface temperature at heat source with different heat fluxes are presented in table 1. The maximum substrate temperature obtained at the heat source by applying different heat fluxes at the bottom wall of the heat sink is compared with the data presented in [53]. The study presented by Vajdi et al.[53] comprises of a similar geometrical structure of a microchannel heat sink having the water as working fluid. The substrate material used in their study is zirconium di-boride (ZrB_2). The data obtained in the present study are compared with the data presented in their research. As can be seen from table 1, the deviation of the data obtained in the present study is 1.1%. So, the data presented in this study agrees quite well with the data presented earlier in literature.

Table 1. Comparison of maximum surface temperature with ZrB_2 as substrate material between the present study and data obtained from [53]

Heat flux at the bottom wall, q" (MW/m^2)	Maximum substrate temperature, present study (K)	Maximum substrate temperature, ref[53] (K)	Deviation
0.9	309.99	308.37	0.52%
1.8	325.55	323.74	0.55%
2.7	342.85	339.10	1.10%
3.6	357.48	354.47	0.85%

One of the key factor to analyze the performance of any heat sink is to observe the heat transfer coefficient of the heat sink. The surface heat transfer coefficient on the bottom wall of the heat sink with three different substrate materials is shown in figure 11. As seen from figure 11, the surface heat transfer coefficient decreases along the channel length from inlet to outlet. This change is seen as the heat transfer coefficient parameter is directly proportional to the temperature difference between the solid and the fluid. Since the temperature of the fluid increases along the flow direction, the temperature difference also gets reduced which results in decreasing the surface heat transfer coefficient. The maximum heat transfer coefficient occurs at the inlet, and the minimum occurs at the outlet of the microchannel. Now, from figure 11, we can clearly see both HfB_2 and TiB_2 show a higher surface heat transfer coefficient at the heat source than that of ZrB_2.

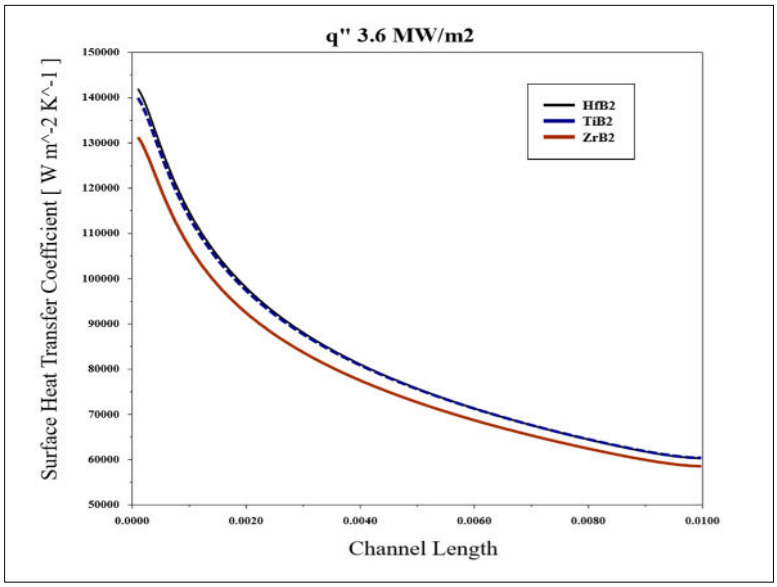

Figure 11. Surface heat transfer coefficient vs. channel length at heat flux 3.6 MW/m^2

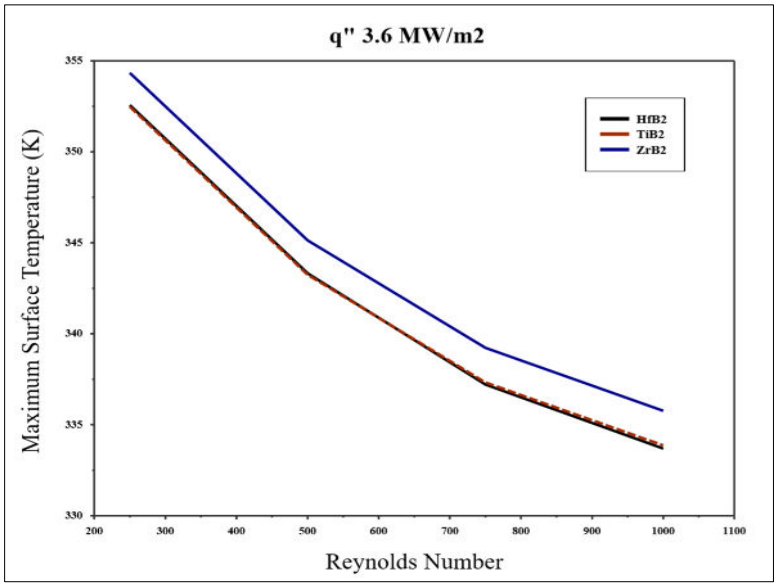

Figure 12. Maximum surface temperature at base vs. Reynolds number

Now, the effect of flow Reynolds number on the overall performance of the heat sink is analyzed. The applied heat flux at the bottom wall of the heat sink is kept 3.6MW/m^2 and the flow Reynolds number is changed from 250 to 1000. The maximum temperature obtained at the heat source with different substrate materials are presented in figure 12. The increase in Reynolds number reduces the maximum surface temperature since it increases the convective heat transfer coefficient from the surface. But by analyzing figure 12, it can be seen that the increase in Reynolds number is not always advantageous. As the decrease in the maximum surface temperature with the increase in Reynolds number does not follow a straight line. Rather, the decrease in maximum surface temperature is less at higher Reynolds number. It can also be seen from figure 12 that, the maximum surface temperature obtained at the heat source is lesser for HfB_2 and TiB_2 substrate materials than ZrB_2.

As mentioned earlier, one of the key parameter to evaluate the performace of any heat sink is to compare the heat transfer coefficient. The maximum surface heat transfer coefficient with three susbtrate materials at different Reynolds number is presented in figure 13. The heat transfer coefficient is calculated at the bottom wall of the microchannel heat sink where the heat flux is applied. It is seen from figure 13 that, the maximum surface heat transfer coefficient is much higher for HfB_2, followed by TiB_2 and ZrB_2.

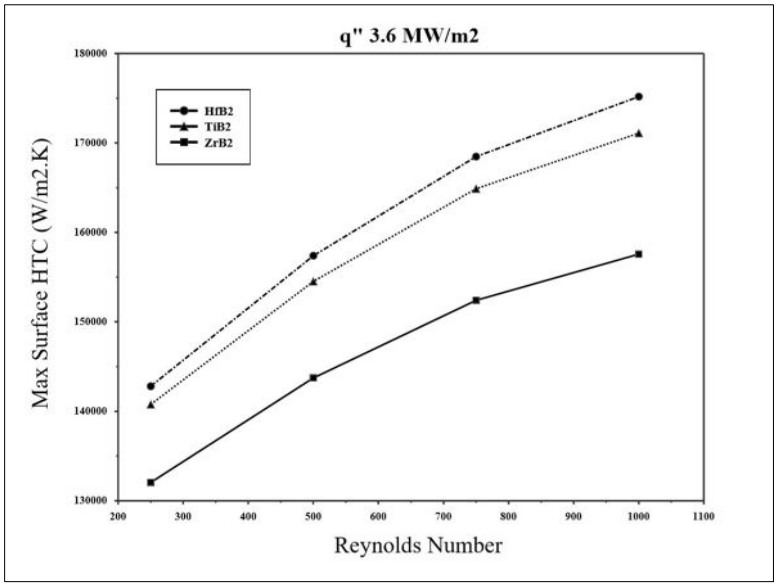

Figure 13. Maximum heat transfer coefficient at heat sink base vs. Reynolds number

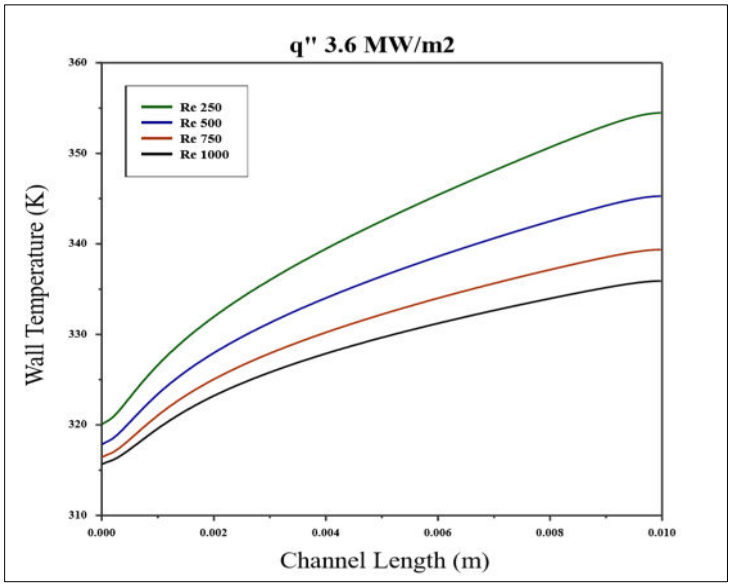

Figure 14. Heat source wall temperature vs. channel length at 3.6 MW/m^2 heat flux at different Reynolds number for ZrB_2

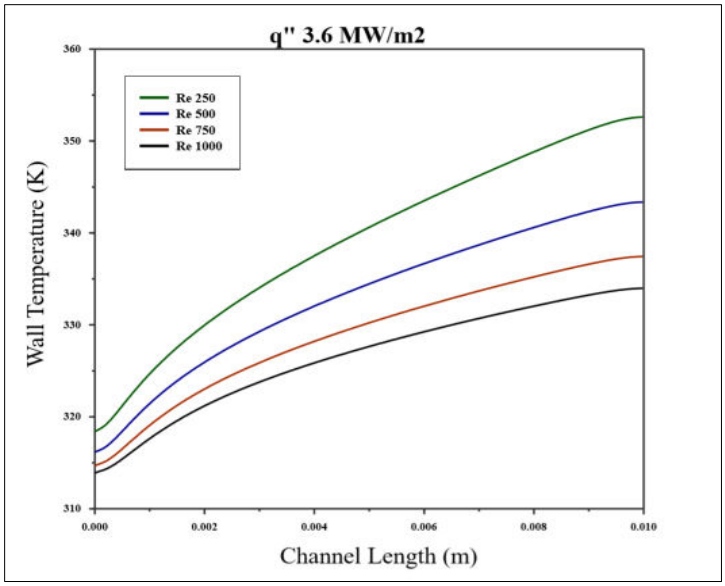

Figure 15. Heat source wall temperature vs. channel length at 3.6 MW/m^2 heat flux at different Reynolds number for TiB_2

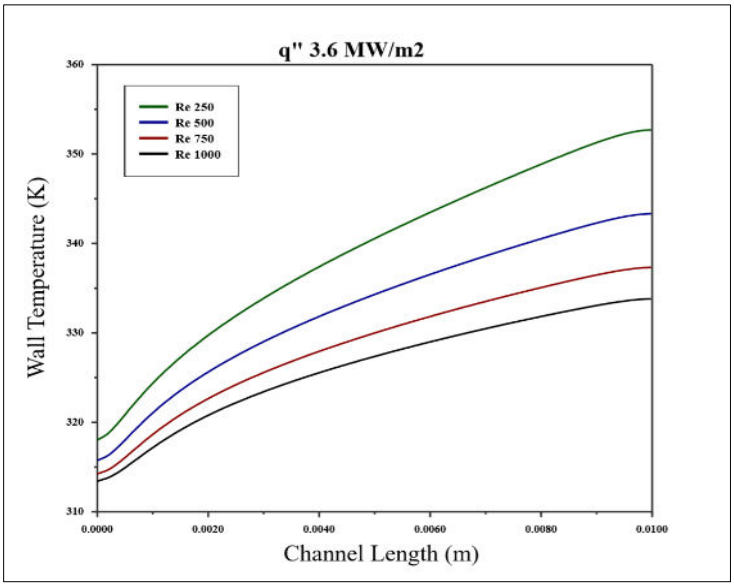

Figure 16. heat source wall temperature vs. channel length at 3.6 MW/m^2 heat flux at different Reynolds number for HfB_2

Finally the effect of flow Reynolds number on the substrate wall temperature is presented in figures 14, 15 and 16. With the increase in flow Rreynolds number, the maximum temperature occurring at the heat source gradually decreases. By analyzing the figures, we can reach to the coclusion that HfB_2 is more efficient in keeping the temperature below a certain point, followed by TiB_2 and lastly ZrB_2. From figures 14, 15, and 16, we can also have a clear idea that the maximum wall temperature of the heat sinks can be kept at a lower value by increasing the flow Reynolds number means increasing the fluid velocity at the inlet. But as we increase the flow Reynolds number more and more, the improvements don't seem to be significant. It might be noted that increased inlet velocity results in higher pressure loss along the flow direction and thus requires more pumping power.

Conclusions

The heat transfer in a microchannel heat sink is numerically analyzed with finite volume method. Water, having a inlet temperature of 273K, is taken as the working fluid. Three different ceramic materials (ZrB_2, TiB_2, and HfB_2) are compared as substrate material for the heat sink. The following conclusions are reached after the present study,

- All of the ceramic materails possess excellent potentialities to be used as a heat transfer agents sue to their higher thermal conductivities and heat capacity values.
- The numerical data obtained in the present study agree well with the data collected from literature.
- Microchannel heat sink (MCHS) can offer high heat transfer coefficients at higher Reynolds number.
- The maximum temperature obtained at the heat source decreases with the increase in Reynolds number.
- Heat sink having substrate materials TiB_2 and HfB_2 show nearly identical performance.
- HfB_2 offers the maximum heat surface heat transfer coefficient followed by TiB_2 and ZrB_2.

The use of ultra-high temperature ceramic materials in microchannel heat sinks can result in significant improvements in heat transfer. As we can see at 3.6 MW/m^2 heat flux, the maximum surface temperature didn't exceed 355K with water as a working fluid. HfB_2 and TiB_2 perform more efficiently than ZrB_2 in obtaining a higher heat transfer coefficient. After watching the heat transfer coefficient for the three materials, we can conclude that HfB_2 and TiB_2 both can be used in microchannel heat sinks. Among these two, HfB_2 shows better heat transfer performance.

References

[1] Z. Qian, Y. Li, Z. Rao, Thermal performance of lithium-ion battery thermal management system by using mini-channel cooling, Energy Convers. Manag. 126 (2016) 622–631. https://doi.org/10.1016/j.enconman.2016.08.063.

[2] M.M. Sarafraz, V. Nikkhah, M. Nakhjavani, A. Arya, Fouling formation and thermal performance of aqueous carbon nanotube nanofluid in a heat sink with rectangular parallel microchannel, Appl. Therm. Eng. 123 (2017) 29–39. https://doi.org/10.1016/j.applthermaleng.2017.05.056.

[3] A.G. Fedorov, R. Viskanta, Three-dimensional conjugate heat transfer in the microchannel heat sink for electronic packaging, Int. J. Heat Mass Transf. 43 (2000) 399–415. https://doi.org/10.1016/S0017-9310(99)00151-9.

[4] D.B. Tuckerman, R.F.W. Pease, D.B. Tuckerman, R.F.W. Pease, High-performance heat sinking for VLSI, IEEE Electron Device Lett. 2 (1981) 126–129. https://doi.org/10.1109/EDL.1981.25367.

[5] P. Gunnasegaran, H.A. Mohammed, N.H. Shuaib, R. Saidur, The effect of geometrical parameters on heat transfer characteristics of microchannels heat sink with different shapes, Int. Commun. Heat Mass Transf. 37 (2010) 1078–1086. https://doi.org/10.1016/j.icheatmasstransfer.2010.06.014.

[6] D.B. Monteiro, P.E.B. de Mello, Thermal performance and pressure drop in a ceramic heat exchanger evaluated using CFD simulations, Energy. 45 (2012) 489–496. https://doi.org/10.1016/j.energy.2012.02.012.

[7] X.J. Shi, S. Li, B. Agnew, Z.H. Zheng, Effects of geometrical parameters and Reynolds number on the heat transfer and flow characteristics of rectangular micro-channel using nano-fluid as working fluid, Therm. Sci. Eng. Prog. 15 (2020). https://doi.org/10.1016/j.tsep.2019.100456.

[8] S.P. Jang, S.U.S. Choi, Cooling performance of a microchannel heat sink with nanofluids, Appl. Therm. Eng. 26 (2006) 2457–2463. https://doi.org/10.1016/j.applthermaleng.2006.02.036.

[9] M. Zadhoush, A. Ahmadi Nadooshan, M. Afrand, H. Ghafori, Constructal optimization of longitudinal and latitudinal rectangular fins used for cooling a plate under free convection by the intersection of asymptotes method, Int. J. Heat Mass Transf. 112 (2017) 441–453. https://doi.org/10.1016/j.ijheatmasstransfer.2017.04.108.

[10] R. Karvinen, T. Karvinen, Optimum geometry of fixed volume plate fin for maximizing heat transfer, Int. J. Heat Mass Transf. 53 (2010) 5380–5385. https://doi.org/10.1016/j.ijheatmasstransfer.2010.07.018.

[11] R. Karvinen, T. Karvinen, Optimum geometry of plate fins, J. Heat Transfer. 134 (2012). https://doi.org/10.1115/1.4006163.

[12] R.. Shah, EXTENDED SURFACE HEAT TRANSFER, A-to-Z Guid. to Thermodyn. Heat Mass Transf. Fluids Eng. e (2006) 1105. https://doi.org/10.1615/AtoZ.e.EXTSURHEATRA.

[13] I.A. Ghani, N.A.C. Sidik, N. Kamaruzaman, Hydrothermal performance of microchannel heat sink: The effect of channel design, Int. J. Heat Mass Transf. 107 (2017) 21–44. https://doi.org/10.1016/j.ijheatmasstransfer.2016.11.031.

[14] G.D. Xia, J. Jiang, J. Wang, Y.L. Zhai, D.D. Ma, Effects of different geometric structures on fluid flow and heat transfer performance in microchannel heat sinks, Int. J. Heat Mass Transf. 80 (2015) 439–447. https://doi.org/10.1016/j.ijheatmasstransfer.2014.08.095.

[15] H.A. Mohammed, P. Gunnasegaran, N.H. Shuaib, Influence of channel shape on the thermal and hydraulic performance of microchannel heat sink, Int. Commun. Heat Mass Transf. 38 (2011) 474–480. https://doi.org/10.1016/j.icheatmasstransfer.2010.12.031.

[16] A. Husain, K.Y. Kim, Shape optimization of micro-channel heat sink for micro-electronic cooling, in: IEEE Trans. Components Packag. Technol., 2008: pp. 322–330. https://doi.org/10.1109/TCAPT.2008.916791.

[17] L. Lin, Y.Y. Chen, X.X. Zhang, X.D. Wang, Optimization of geometry and flow rate distribution for double-layer microchannel heat sink, Int. J. Therm. Sci. 78 (2014) 158–168. https://doi.org/10.1016/j.ijthermalsci.2013.12.009.

[18] S.H. Chong, K.T. Ooi, T.N. Wong, Optimisation of single and double layer counter flow microchannel heat sinks, Appl. Therm. Eng. 22 (2002) 1569–1585. https://doi.org/10.1016/S1359-4311(02)00083-2.

[19] A. Sakanova, S. Yin, J. Zhao, J.M. Wu, K.C. Leong, Optimization and comparison of double-layer and double-side micro-channel heat sinks with nanofluid for power electronics cooling, Appl. Therm. Eng. 65 (2014) 124–134. https://doi.org/10.1016/j.applthermaleng.2014.01.005.

[20] G. Xie, Z. Chen, B. Sunden, W. Zhang, Numerical predictions of the flow and thermal performance of water-cooled single-layer and double-layer wavy microchannel heat sinks, Numer. Heat Transf. Part A Appl. 63 (2013) 201–225. https://doi.org/10.1080/10407782.2013.730445.

[21] K. Jeevan, I.A. Azid, K.N. Seetharamu, Optimization of double layer counter flow (DLCF) micro-channel heat sink used for cooling chips directly, in: Proc. 6th Electron. Packag. Technol. Conf. EPTC 2004, 2004: pp. 553–558. https://doi.org/10.1109/eptc.2004.1396669.

[22] K.C. Wong, M.L. Ang, Thermal hydraulic performance of a double-layer microchannel heat sink with channel contraction, Int. Commun. Heat Mass Transf. 81 (2017) 269–275. https://doi.org/10.1016/j.icheatmasstransfer.2016.09.013.

[23] Y. Hadad, B. Ramakrishnan, R. Pejman, S. Rangarajan, P.R. Chiarot, A. Pattamatta, B. Sammakia, Three-objective shape optimization and parametric study of a micro-channel heat sink with discrete non-uniform heat flux boundary conditions, Appl. Therm. Eng. (2019) 720–737. https://doi.org/10.1016/j.applthermaleng.2018.12.128.

[24] P. Nitiapiruk, O. Mahian, A.S. Dalkilic, S. Wongwises, Performance characteristics of a microchannel heat sink using TiO2/water nanofluid and different thermophysical models, Int. Commun. Heat Mass Transf. 47 (2013) 98–104. https://doi.org/10.1016/j.icheatmasstransfer.2013.07.001.

[25] T.H. Tsai, R. Chein, Performance analysis of nanofluid-cooled microchannel heat sinks, Int. J. Heat Fluid Flow. 28 (2007) 1013–1026. https://doi.org/10.1016/j.ijheatfluidflow.2007.01.007.

[26] E.M. Tokit, H.A. Mohammed, M.Z. Yusoff, Thermal performance of optimized interrupted microchannel heat sink (IMCHS) using nanofluids, Int. Commun. Heat Mass Transf. 39 (2012) 1595–1604. https://doi.org/10.1016/j.icheatmasstransfer.2012.10.013.

[27] A.A. Awais, M.H. Kim, Experimental and numerical study on the performance of a minichannel heat sink with different header geometries using nanofluids, Appl. Therm. Eng. 171 (2020). https://doi.org/10.1016/j.applthermaleng.2020.115125.

[28] A. Muhammad, D. Selvakumar, J. Wu, Numerical investigation of laminar flow and heat transfer in a liquid metal cooled mini-channel heat sink, Int. J. Heat Mass Transf. 150 (2020) 119265. https://doi.org/10.1016/j.ijheatmasstransfer.2019.119265.

[29] A. Muhammad, D. Selvakumar, A. Iranzo, Q. Sultan, J. Wu, Comparison of pressure drop and heat transfer performance for liquid metal cooled mini-channel with different coolants and heat sink materials, J. Therm. Anal. Calorim. (2020). https://doi.org/10.1007/s10973-020-09318-2.

[30] S.-W. Kang, L.J. Yang, C.-S. Yu, J.-S. Chen, Performance test and analysis of silicon-based microchannel heat sink, in: R.J. Hwu, K. Wu (Eds.), Terahertz and Gigahertz Photonics, SPIE, 1999: p. 259. https://doi.org/10.1117/12.370172.

[31] V.V. Kuznetsov, A.S. Shamirzaev, Flow Boiling Heat Transfer of Refrigerant R-134a in Copper Microchannel Heat Sink, in: Heat Transf. Eng., Taylor and Francis Ltd., 2016: pp. 1105–1113. https://doi.org/10.1080/01457632.2015.1111103.

[32] T. Dang, N. Tran, J.T. Teng, Numerical and experimental investigations on heat transfer phenomena of an aluminium microchannel heat sink, Appl. Mech. Mater. 145 (2012) 129–133. https://doi.org/10.4028/www.scientific.net/AMM.145.129.

[33] A. Zadra, G. Robert, Dream recall frequency: Impact of prospective measures and motivational factors, Conscious. Cogn. 21 (2012) 1695–1702. https://doi.org/10.1016/j.concog.2012.08.011.

[34] A. Traverso, A.F. Massardo, R. Scarpellini, Externally Fired micro-Gas Turbine: Modelling and experimental performance, Appl. Therm. Eng. 26 (2006) 1935–1941. https://doi.org/10.1016/j.applthermaleng.2006.01.013.

[35] A. Sabahi Namini, A. Motallebzadeh, B. Nayebi, M. Shahedi Asl, M. Azadbeh, Microstructure–mechanical properties correlation in spark plasma sintered Ti–4.8 wt.% TiB2 composites, Mater. Chem. Phys. 223 (2019) 789–796. https://doi.org/10.1016/j.matchemphys.2018.11.057.

[36] K.A. Al-attab, Z.A. Zainal, Performance of high-temperature heat exchangers in biomass fuel powered externally fired gas turbine systems, Renew. Energy. 35 (2010) 913–920. https://doi.org/10.1016/j.renene.2009.11.038.

[37] E. Zapata-Solvas, D.D. Jayaseelan, H.T. Lin, P. Brown, W.E. Lee, Mechanical properties of ZrB2- and HfB2-based ultra-high temperature ceramics fabricated by spark plasma sintering, J. Eur. Ceram. Soc. 33 (2013) 1373–1386. https://doi.org/10.1016/j.jeurceramsoc.2012.12.009.

[38] F. Monteverde, Ultra-high temperature HfB2-SiC ceramics consolidated by hot-pressing and spark plasma sintering, J. Alloys Compd. 428 (2007) 197–205. https://doi.org/10.1016/j.jallcom.2006.01.107.

[39] R. Königshofer, S. Fürnsinn, P. Steinkellner, W. Lengauer, R. Haas, K. Rabitsch, M. Scheerer, Solid-state properties of hot-pressed TiB2 ceramics, in: Int. J. Refract. Met. Hard Mater., Elsevier, 2005: pp. 350–357. https://doi.org/10.1016/j.ijrmhm.2005.05.006.

[40] F. Sadegh Moghanlou, M. Vajdi, J. Sha, A. Motallebzadeh, M. Shokouhimehr, M. Shahedi Asl, A numerical approach to the heat transfer in monolithic and SiC reinforced HfB2, ZrB2 and TiB2 ceramic cutting tools, Ceram. Int. 45 (2019) 15892–15897. https://doi.org/10.1016/j.ceramint.2019.05.095.

[41] T. Ai, F. Wang, X. Feng, M. Ruan, Microstructural and mechanical properties of dual Ti3AlC 2-Ti2AlC reinforced TiAl composites fabricated by reaction hot pressing, Ceram. Int. 40 (2014) 9947–9953. https://doi.org/10.1016/j.ceramint.2014.02.092.

[42] M. Vajdi, F. Sadegh Moghanlou, Z. Ahmadi, A. Motallebzadeh, M. Shahedi Asl, Thermal diffusivity and microstructure of spark plasma sintered TiB 2 [sbnd]SiC[sbnd]Ti composite, Ceram. Int. 45 (2019) 8333–8344. https://doi.org/10.1016/j.ceramint.2019.01.141.

[43] Z. Saleem, H. Rennebaum, F. Pudel, E. Grimm, Treating bast fibres with pectinase improves mechanical characteristics of reinforced thermoplastic composites, Compos. Sci. Technol. 68 (2008) 471–476. https://doi.org/10.1016/j.compscitech.2007.06.005.

[44] R.J. Kee, B.B. Almand, J.M. Blasi, B.L. Rosen, M. Hartmann, N.P. Sullivan, H. Zhu, A.R. Manerbino, S. Menzer, W.G. Coors, J.L. Martin, The design, fabrication, and evaluation of a ceramic counter-flow microchannel heat exchanger, Appl. Therm. Eng. 31 (2011) 2004–2012. https://doi.org/10.1016/j.applthermaleng.2011.03.009.

[45] M. Sakkaki, F. Sadegh Moghanlou, M. Vajdi, F.Z. Pishgar, M. Shokouhimehr, M. Shahedi Asl, The effect of thermal contact resistance on the temperature distribution in a WC made cutting tool, Ceram. Int. 45 (2019) 22196–22202. https://doi.org/10.1016/j.ceramint.2019.07.241.

[46] M. Mallik, A.J. Kailath, K.K. Ray, R. Mitra, Electrical and thermophysical properties of ZrB 2 and HfB 2 based composites, J. Eur. Ceram. Soc. 32 (2012) 2545–2555. https://doi.org/10.1016/j.jeurceramsoc.2012.02.013.

[47] J.W. Zimmermann, G.E. Hilmas, W.G. Fahrenholtz, R.B. Dinwiddie, W.D. Porter, H. Wang, Thermophysical Properties of ZrB_2 and ZrB_2 –SiC Ceramics, J. Am. Ceram. Soc. 91 (2008) 1405–1411. https://doi.org/10.1111/j.1551-2916.2008.02268.x.

[48] S.Q. Guo, Densification of ZrB2-based composites and their mechanical and physical properties: A review, J. Eur. Ceram. Soc. 29 (2009) 995–1011. https://doi.org/10.1016/j.jeurceramsoc.2008.11.008.

[49] M. Khoeini, A. Nemati, M. Zakeri, M. Shahedi Asl, Pressureless sintering of ZrB 2 ceramics codoped with TiC and graphite, Int. J. Refract. Met. Hard Mater. 81 (2019) 189–195. https://doi.org/10.1016/j.ijrmhm.2019.02.026.

[50] M. Shahedi Asl, Y. Azizian-Kalandaragh, Z. Ahmadi, A. Sabahi Namini, A. Motallebzadeh, Spark plasma sintering of ZrB2-based composites co-reinforced with SiC whiskers and pulverized carbon fibers, Int. J. Refract. Met. Hard Mater. 83 (2019) 104989. https://doi.org/10.1016/j.ijrmhm.2019.104989.

[51] N. Pourmohammadie Vafa, M. Ghassemi Kakroudi, M. Shahedi Asl, Advantages and disadvantages of graphite addition on the characteristics of hot-pressed ZrB2–SiC composites, Ceram. Int. 46 (2020) 8561–8566. https://doi.org/10.1016/j.ceramint.2019.12.086.

[52] S. Nekahi, M. Vajdi, F. Sadegh Moghanlou, K. Vaferi, A. Motallebzadeh, M. Özen, U. Aydemir, J. Sha, M. Shahedi Asl, TiB2–SiC-based ceramics as alternative efficient micro heat exchangers, Ceram. Int. 45 (2019) 19060–19067. https://doi.org/10.1016/j.ceramint.2019.06.150.

[53] M. Vajdi, F. Sadegh Moghanlou, E. Ranjbarpour Niari, M. Shahedi Asl, M. Shokouhimehr, Heat transfer and pressure drop in a ZrB2 microchannel heat sink: A numerical approach, Ceram. Int. 46 (2020) 1730–1735. https://doi.org/10.1016/j.ceramint.2019.09.146.

[54] F. Sadegh, M. Vajdi, A. Motallebzadeh, J. Sha, Numerical analyses of heat transfer and thermal stress in a ZrB 2 gas turbine stator blade, Ceram. Int. 45 (2019) 17742–17750. https://doi.org/10.1016/j.ceramint.2019.05.344.

[55] S. Nekahi, K. Vaferi, M. Vajdi, F. Sadegh Moghanlou, M. Shahedi Asl, M. Shokouhimehr, A numerical approach to the heat transfer and thermal stress in a gas turbine stator blade made of HfB2, Ceram. Int. 45 (2019) 24060–24069. https://doi.org/10.1016/j.ceramint.2019.08.112.

[56] S.A. Delbari, A. Sabahi Namini, M. Shahedi Asl, Hybrid Ti matrix composites with TiB2 and TiC compounds, Mater. Today Commun. 20 (2019) 100576. https://doi.org/10.1016/j.mtcomm.2019.100576.

[57] P. Fallahazad, N. Naderi, M.J. Eshraghi, A. Massoudi, Optimization of Chemical Texturing of Silicon Wafers Using Different Concentrations of Sodium Hydroxide in Etching Solution, Adv. Ceram. Prog. 3 (2017) 16–18. https://doi.org/10.30501/ACP.2017.90753.

[58] F. Shayesteh, S.A. Delbari, Z. Ahmadi, M. Shokouhimehr, M. Shahedi Asl, Influence of TiN dopant on microstructure of TiB2 ceramic sintered by spark plasma, Ceram. Int. 45 (2019) 5306–5311. https://doi.org/10.1016/j.ceramint.2018.11.228.

[59] L. Zhang, D.A. Pejaković, J. Marschall, M. Gasch, Thermal and Electrical Transport Properties of Spark Plasma-Sintered HfB2 and ZrB2 Ceramics, J. Am. Ceram. Soc. 94 (2011) 2562–2570. https://doi.org/10.1111/j.1551-2916.2011.04411.x.

[60] J.W. Lawson, C.W. Bauschlicher, M.S. Daw, Ab Initio Computations of Electronic, Mechanical, and Thermal Properties of ZrB 2 and HfB 2, J. Am. Ceram. Soc. 94 (2011) 3494–3499. https://doi.org/10.1111/j.1551-2916.2011.04649.x.

[61] E. Wuchina, M. Opeka, S. Causey, K. Buesking, J. Spain, A. Cull, J. Routbort, F. Guitierrez-Mora, Designing for ultrahigh-temperature applications: The mechanical and thermal properties of HfB2, HfCx, HfNx and αHf(N), in: J. Mater. Sci., Springer, 2004: pp. 5939–5949. https://doi.org/10.1023/B:JMSC.0000041690.06117.34.

[62] B.G. Carman, J.S. Kapat, L.C. Chow, L. An, Impact of a ceramic microchannel heat exchanger on a micro turbine, in: Am. Soc. Mech. Eng. Int. Gas Turbine Institute, Turbo Expo IGTI, American Society of Mechanical Engineers Digital Collection, 2002: pp. 1053–1060. https://doi.org/10.1115/GT2002-30544.

[63] V. Nagarajan, Y. Chen, Q. Wang, T. Ma, Hydraulic and thermal performances of a novel configuration of high temperature ceramic plate-fin heat exchanger, Appl. Energy. 113 (2014) 589–602. https://doi.org/10.1016/j.apenergy.2013.07.037.

[64] M. Fattahi, K. Vaferi, M. Vajdi, F. Sadegh Moghanlou, A. Sabahi Namini, M. Shahedi Asl, Aluminum nitride as an alternative ceramic for fabrication of microchannel heat exchangers: A numerical study, Ceram. Int. (2020) 0–1. https://doi.org/10.1016/j.ceramint.2020.01.195.

[65] P. Bhattacharya, A.N. Samanta, S. Chakraborty, Numerical study of conjugate heat transfer in rectangular microchannel heat sink with Al2O3/H2O nanofluid, Heat Mass Transf. Und Stoffuebertragung. 45 (2009) 1323–1333. https://doi.org/10.1007/s00231-009-0510-0.

[66] F. Nakamori, Y. Ohishi, H. Muta, K. Kurosaki, K. Fukumoto, S. Yamanaka, Mechanical and thermal properties of bulk ZrB2, J. Nucl. Mater. 467 (2015) 612–617. https://doi.org/10.1016/j.jnucmat.2015.10.024.

[67] R.G. Munro, Material properties of titanium diboride, J. Res. Natl. Inst. Stand. Technol. 105 (2000) 709. https://doi.org/10.6028/jres.105.057.